December, 1998

Experimental Study on Electric-Current Induced Damage Evolution at the Crack Tip in Thin Film Conductors

Ashraf F. Bastawros, *Harvard University*
K.-S. Kim, *Brown University*

Experimental Study on Electric-Current Induced Damage Evolution at the Crack Tip in Thin Film Conductors

A.-F. Bastawros
Division of Engineering and Applied Science,
Harvard University,
ESL, 40 Oxford Street,
Cambridge, MA 02138

K.-S. Kim
Division of Engineering,
Brown University,
Providence, RI 02912

The time dependent temperature distribution induced by electric current heating in a double edge cracked, unpassivated thin aluminum or gold film interconnect lines is monitored using a high resolution infrared imaging system. A pure aluminum or gold film, with a thickness of 0.2 μm, is deposited by high vacuum evaporation coating and patterned into test structures of varying widths. The operative mechanisms of mass transport are assessed in view of the monitored temperature profile. The precracked aluminum film shows fine crack growth towards the positive electrode, which originates from the initial crack tips. The crack-tip temperature is close to melting, during propagation. After the initial crack propagation, a hot spot is formed between the two elongated cracks, and leads to failure. The crack growth generates a backward mass flow towards the negative electrode. The gold film shows a different pattern, in which the original cracks propagate towards each other with a slight tilt towards the negative electrode. The tip temperature is lower than the melting temperature. These time dependent failure mechanisms are rationalize using a proposed critical current intensity factor and a normalized current intensity rate, similar to the fracture toughness K_{IC} for brittle fracture.

1 Introduction

Interconnect lines always contain variety of preexisting defects such as voids and cracks. These defects become the origin of local hot spots, which have a major role in controlling the driving forces for the different micromechanisms of interconnect line failures. Both the geometry of the line and the material microstructure further control the driving forces for the growth of flaws (Attardo et al., 1970). For example, higher grain size to line width ratio (the quasi-bamboo structure) improves the mean time to failure. To shed some light on such a failure process, this paper presents an experimental study of the roles of electric-current (EC) induced damage around preexisting flaws in the interconnect line. While a typical interconnect line has a dimension of the order ~1 μm, we implement a larger macroscopic representative configuration of a precracked unpassivated film, with a line width of several hundred microns, to provide macroscopic observation of the failure process (Fig. 1). Moreover, this experimental configuration is adopted to monitor the spatial distribution of temperature around the crack tip by a high resolution infrared camera. The final failure morphology is studied by the aid of an Atomic Force Microscope (AFM). The failure process has been studied in aluminum and gold films.

The micromechanisms of these failure processes are governed by the kinetics of inhomogeneous diffusions and/or reactions. These mechanisms are electromigration, thermally assisted diffusion (Soret diffusion), diffusion driven by stress gradients, and diffusion driven by surface tension gradients. The electronic band structure of the conductor, together with the associated transport mechanisms, set both the magnitude and the sign of the atomic/vacancy flux for the kinetic process. For example, atoms move towards the positive electrode in a uniform aluminum (Al) test line and generate voids towards the negative electrode, at a rate approximately proportional to the current density for a wide range of testing temperatures (Gardner et al., 1987). The diffusion rates become highly nonuniform around preexisting flaws within the line microstructure, and under the presence of the local temperature gradient. The effect of electromigration as well as the variation of diffusion rates will accelerate void growth and translation, and the accompanied stress buildups, leading to a final failure of the interconnect line (Ho, 1970; Marieb et al., 1994).

Near a crack tip, the mentioned micromechanisms of failure are affected by the mutual interaction of simultaneous fluxes of charge, heat, and mass/vacancies. This problem of a precracked thin film under EC has been studied for decades. Within a homogenous framework, Sigsbee (1973) showed that the increase of the localized temperature due to Joule heating promotes vacancy migration towards the crack tip along grain boundaries. Saka et al. (1994) considered the effect of heat generation or absorption due to Thomson effect on the near tip temperature distribution and as a competing driving force in Soret diffusion. We showed in an earlier study (Bastawros and Kim, 1995) that an existing crack normal to an aluminum line propagates towards the positive electrode (in contrast to simple electromigration) until an extended damage zone sweeps the whole line cross section. For the case of a gold (Au) line (Bastawros and Kim, 1997), the crack propagates normal to the line, forming a slit-like failure. These two particular metal conductors have different electronic band structures, which respond to driving potentials (e.g., voltage, temperature, . . . etc.) in different ways. As a continuum failure criterion, we (1995) proposed a macroscopic critical-current intensity factor, K^*, to be used as a material property governing failures under EC loading; analogous to the fracture toughness K_{IC} for brittle fracture. Our experimental results showed that the morphology of failure or the pattern of damage evolution depends strongly on the EC loading rate (or the current intensity rate $\dot{K}^*$) and the ligament width.

Contributed by the Electrical and Electronic Packaging Division for publication in the JOURNAL OF ELECTRONIC PACKAGING. Manuscript received by the EEPD January 15, 1998; revision received August 15, 1998. Associate Technical Editor: D. T. Read.

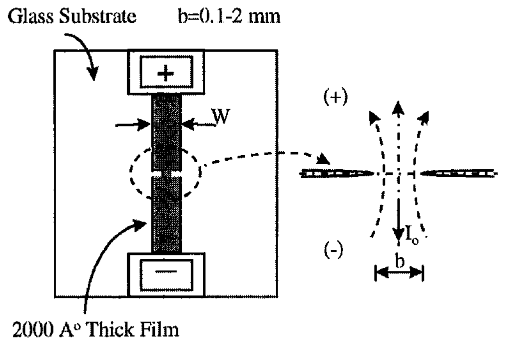

Fig. 1 Specimen configuration

This paper presents additional details for the EC-loading-rate-dependent failure of precracked Al and Au films at a particular range of $\dot{K}^* \cong 5$ kA/cm$^{3/2}$s that induces initial crack propagation. The continuum failure criterion as well as the corresponding time dependent failure are discussed in section 2. A summary of the experimental procedure and measurements is outlined in section 3. All experimental observations and the monitored time dependent temperature distribution around the crack tip are given in section 4. In the final section, the measured temperature field is used in conjunction with an energy argument to predict the dominant driving forces near a crack tip, and then to explain the difference in the observed damage and the crack growth direction.

2 Continuum Failure Criterion

In the presence of a crack tip, the nominal current density of the current flux normal to the prospective crack plane, $\mathbf{j}$, has an inverse square root dependence with respect to distance from the crack tip, Fig. 1 (Bastawros and Kim, 1995). Furthermore, the critical current to failure depends on the uncracked ligament width in a manner similar to that of brittle fracture. Therefore, the onset of failure is reached when K^* (current intensity factor) reaches a critical value K_C^* (current toughness). The total current, I_{OC}, that can be transmitted through a given ligament of width b is predicted as

$$\frac{I_{OC}}{h} = K_C^* \sqrt{\frac{\pi b}{2}}, \qquad (1)$$

where h is the line thickness. The ratio b/w must be much smaller than unity, where w is the total width. The experimental measurements show that Eq. (1) is satisfied for both Al and Au film materials. K_C^* is estimated with a best fit for Eq. (1), as 0.16 MA/cm$^{3/2}$ for Al and 0.125 MA/cm$^{3/2}$ for Au. The prediction of Eq. (1) is plotted in Fig. 2 and concurred with the experimental data. Moreover, for the Al-film, the nominal current at a nominal microstructure distance of 0.1 μm (the typical grain size of the tested film) from the crack tip is estimated with the singular term, and its density turns out to be approximately 20 MA/cm^2. This value has the same order of magnitude as the limit current density of a single crystal Al line, which is reported by Kaneko et al. (1994) as 35 MA/cm^2.

The failure characteristics of a cracked line under time dependent EC loading has shown a strong dependence on the rate at which the EC is applied (or the current intensity rate $\dot{K}^*$). The observed morphology of failures is shown in Fig. 3, and can be classified as function of $\dot{K}^*$ into three categories. For $\dot{K}^* \cong$ 0.5 kA/cm$^{3/2}$s, a spread failure occurs within the uncracked ligament, with no crack propagation, Fig. 3(*a*). For $\dot{K}^* \cong 5$ kA/cm$^{3/2}$s, minor crack propagation occurs, followed by a spread failure, Fig. 3(*b*). For $\dot{K}^* \geq 100$ kA/cm$^{3/2}$s, a very localized failure mode takes place with melting of the uncracked ligament, Fig. 3(*c*). The observed failure modes are consistent for all tested lines, regardless of the uncracked ligament width or misalignment of the two notches.

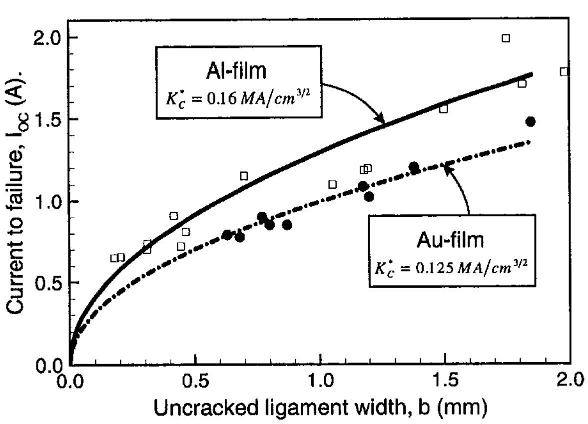

Fig. 2 Dependence of critical failure current on the uncracked ligament width

3 Experimental Procedures

A 0.2 μm thick layer of either Al or Au is deposited by high vacuum thermal evaporation coating on a Soda-lime glass sub-

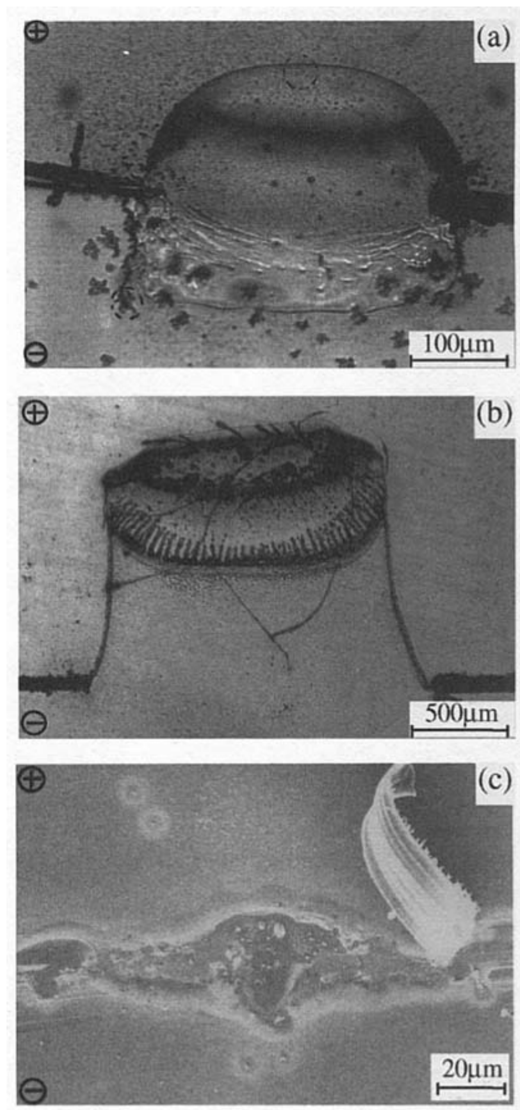

Fig. 3 The different rate-dependent failures: (*a*) spread failure, $\dot{K}^* \cong 0.5kA/cm^{3/2}s$; (*b*) spread failure with minor crack propagation, $\dot{K}^* \cong 5kA/cm^{3/2}s$; and (*c*) localized failure, $\dot{K}^* \geq 100kA/cm^{3/2}s$

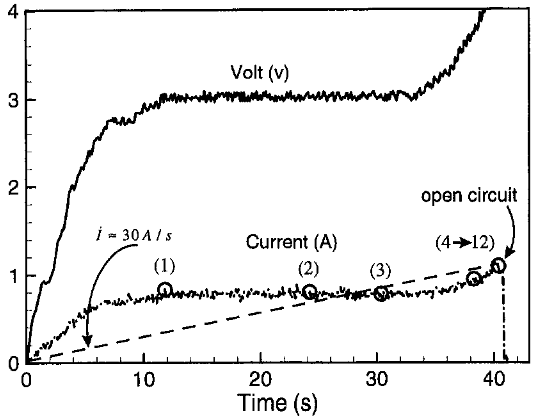

Fig. 4 A typical time-history profiles for voltage and applied EC. The numbers mark the corresponding time for the IR images in Fig. 5.

strate. The average grain size is 0.1–0.15 μm. The tested line dimensions are 25 mm long and 10 mm wide (Fig. 1). Fine slit-like cracks of 15 μm width are scribed into the test lines. The uncracked ligament width is varied between 0.1–2.0 mm.

Temperature distribution around the crack tip is monitored through a high resolution infrared (IR) camera (Amber–Galileo) with a 256 × 256 array and a 30 μm pixel size. An IR microscope lens is used to provide 1× magnification. The high reflectivity and low emissivity (<0.05) of the tested film increases the narcissistic effect (the detector thermal energy is reflected by the film surface), and induces an uneven imaging of cracked region. Therefore, the ambient thermal radiation is captured before passing the electric current and thereafter, subtracted from each IR image. This procedure is facilitated by using a fast camera frame rate (130 frames/s) in conjunction with a short integration time (15 μs). The IR images are captured at a rate of 16 frames/s employing the EchoTherm digital control system (*EchoTherm Manual,* 1997). The digital IR images are post-processed using Planck's radiation law. In this calibration, the possible changes of surface emissivity is ignored. The calibration has been carried by uniformly heating the same substrate-film combination up to 450°C for the Al film and up to 550°C for the Au film. Any reported temperatures, above the calibration range, are based on extrapolating the calibration relationships.

A voltage-controlled power supply, monitored by a current probe, is used to provide an electrical current across the test line. The EC is applied in a slow ramping of approximately 30–50 mA/s until failure ($\dot{K}^* \cong 5$ kA/cm$^{3/2}$s) to induce minor crack propagation and spread failure within the uncracked ligament. The analog signals of current and voltage are fed to an A/D converter board, and then to a personal computer for recording through a virtual instrument generated by a LabView program. The virtual instrument synchronizes the measurements with the recorded IR images. Typical failure cases are presented separately below for both Al and Au films.

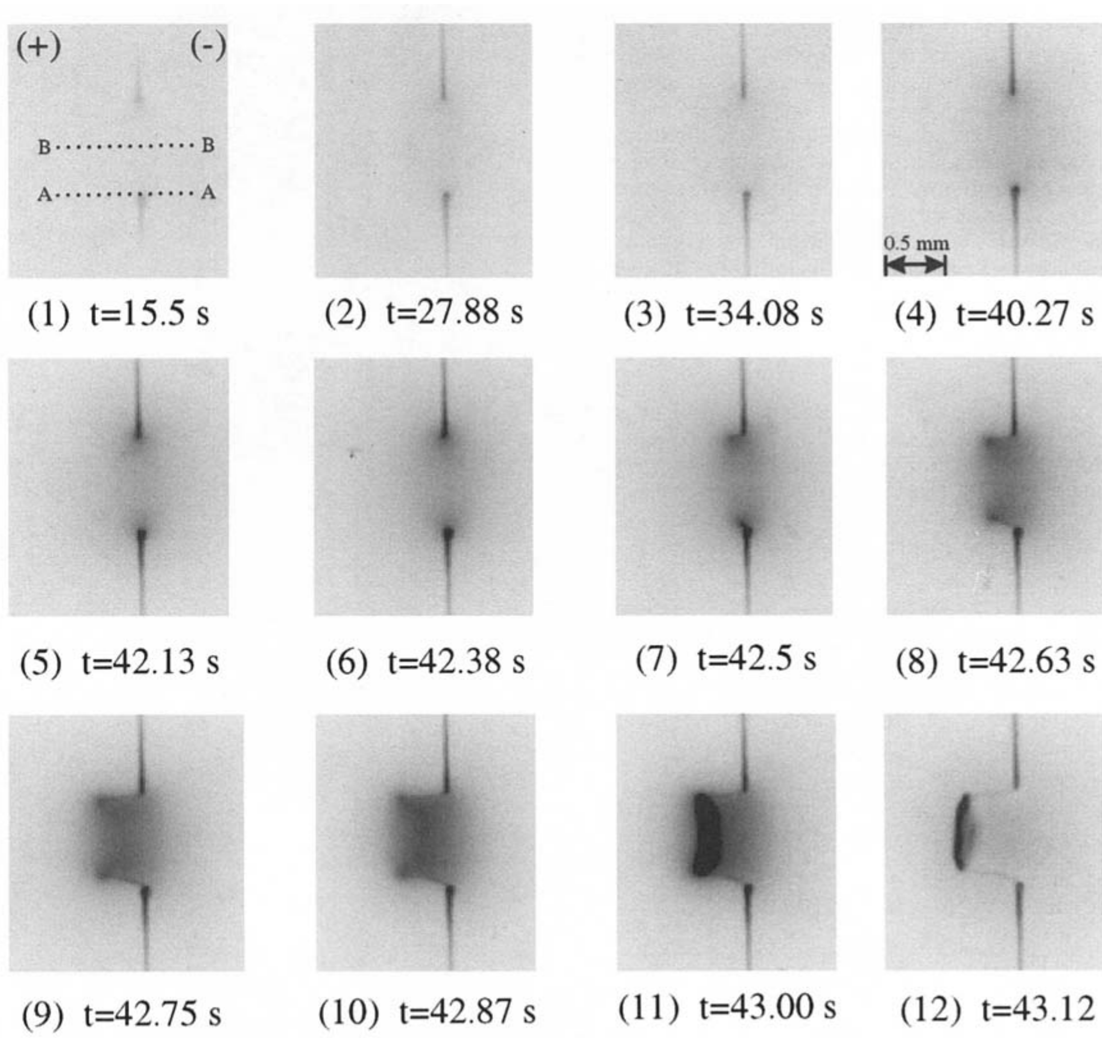

Fig. 5 IR images for the time dependent temperature distribution induced by EC loading in Al-line

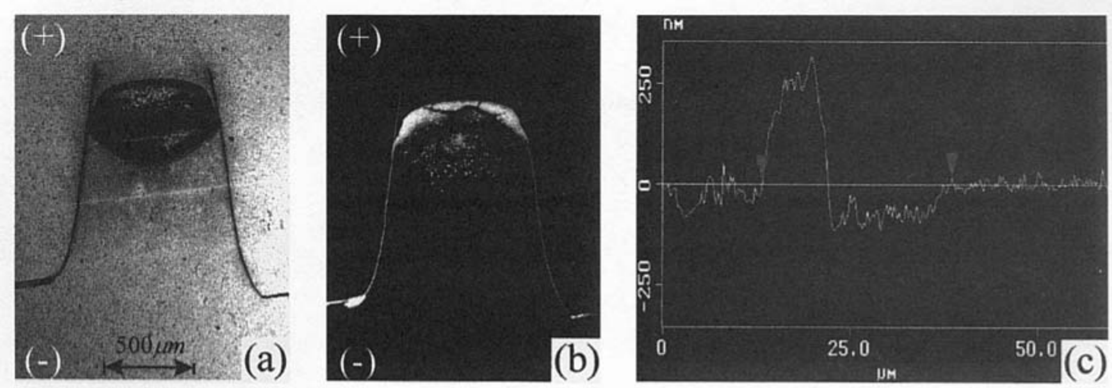

Fig. 6 Localized crack propagation in Al-film with a final spread failure: (*a*) reflected optical image; (*b*) transmitted optical image; and (*c*) AFM thickness profile across the right side of the propagating crack (Fig. 6(*a*))

4 Experimental Results

4.1 Aluminum Film. A typical time history profile of an Al film is shown in Fig. 4 for the voltage and applied current to failure. The corresponding IR images are presented in Fig. 5. This sequence of IR images indicates that the failure process occurs in three consecutive steps. First, a hot spot is formed ahead of the crack tip and grows as the current increases (Fig. 5 (1:6)). Second, a fine crack starts to grow in a curved trajectory towards the positive electrode for over a second (Fig. 5 (7:10)). Third, an extended hot spot is formed between the two crack flanks and melts the remaining ligament in less than 50 ms (Fig. 5 (11:12)). Figure 6 shows typical cases of the final failure for the double edge cracked Al lines. In some cases, the crack either propagates beyond the melting zone (Fig. 6(*a, b*)) or terminates at this zone. Figure 6(*c*) is an AFM thickness profile across the crack. It clearly shows a sharp ridge and accumulation of material towards the original crack plane. This material accumulation is in the opposite direction to the electron flow. An extended zone of 5 μm diameter voids is also observed to surround the propagating cracks. These voids presumably do not reach the substrate, since they are not visible in an optical transmission microscope. The exact topography of these voids has been analyzed by the AFM.

Figure 7(*a*) and 7(*b*) represent, respectively, the time dependent temperature distribution on lines A–A perpendicular to the crack direction and on line B–B passing through the midpoint of the uncracked ligament (Fig. 5(1)). In this figure, each curve (noted by a number) represents the spatial temperature distribution at a particular instant, which corresponds to Fig. 5. These measurements presents a striking results, if one notices that the temperature profiles lose their symmetry around the crack plane and extend towards the positive electrode before the start of crack propagation. The temperature of the whole region (within 3 mm) around the crack plane has reached 150°C, and probably close to melting within the failure zone (T_m = 660°C). The tip temperature may have reached the melting point just before propagation (Fig. 5 (6)). However, care should be taken when interpreting the temperature of the crack tip. Surface emissivity might have changed at such high temperature due to surface oxidation and void growth in the vicinity of the crack tip.

4.2 Gold Film. The Au lines showed very different behavior from the Al lines. The IR images (Fig. 8) show singular temperature distribution around each crack tip. This localized temperature distribution rises as the EC increases until a sharp crack starts to propagate from each tip. In less than 50 ms, the two cracks begin to grow in slightly tilted trajectories towards the negative electrode until they join together and form a narrow melted spot. Figure 9 shows reflected and transmitted optical micrographs for the spread failure zone. Voids are nucleated and grown in the vicinity of the crack plane. Similar to Al case, the voids do not reach the substrate.

Figure 10(*a*) and 10(*b*) represents, respectively, the time dependent temperature distributions on lines A–A and B–B of Fig. 8 (1). The temperature profiles seem to be symmetrically distributed around the crack plane. The tip temperature may have reached the melting point (T_m = 1064°C) within a very

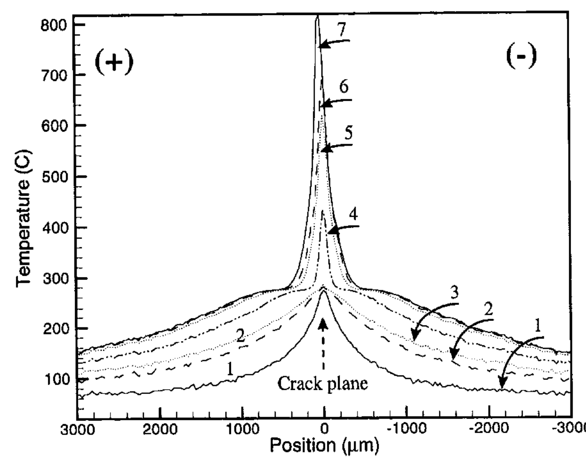

(a)

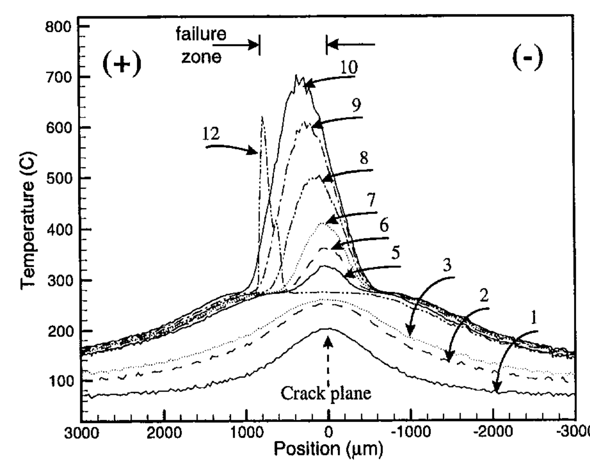

(b)

Fig. 7 Time dependent temperature distribution in A1-film: (*a*) tip temperature profile at line A-A of Fig. 5 up to the onset of crack propagation; and (*b*) middle plane temperature profile at line B-B of Fig. 5 up to the final failure

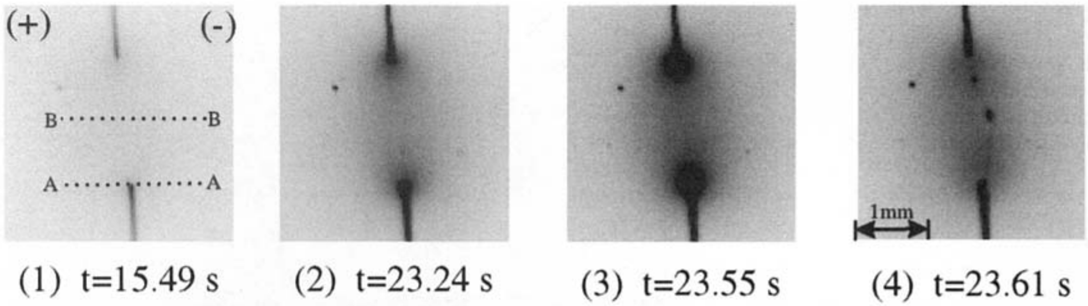

Fig. 8 IR images for the time dependent distribution induced by EC loading in Au-line

localized region. However, the middle plane temperature distribution does not show temperature increase above 400°C.

5 Discussion and Conclusion

The failure process of an interconnect line arises from the mutual interaction of the following three simultaneous fluxes within the line: charge flux, heat flux, and mass/vacancies flux. The flow of the EC current induces not only a charge flux but also heat and mass fluxes. Two different heating mechanisms control the heat flux within the interconnect line. The first one is the irreversible Joule heating which arises from the electrical resistance of the film. The second one is the reversible Thomson heating which arises from the EC flow in a temperature gradient and has the same order as Joule heating (Adkins, 1983). Both the EC and heat flux will control the mass flux in the form of electromigration and thermally assisted diffusion. The following section outlines the nature of these fluxes near a crack tip.

In the presence of a current flux, both Thomson and Joule heating will prevail and the associated temperature field (around the crack tip) must satisfy the energy conservation:

$$\rho|\mathbf{j}|^2 + \eta\mathbf{j}\cdot\nabla T - \lambda\nabla^2 T - C\partial T/\partial t = 0. \qquad (2)$$

Here, ∇ is the spatial gradient operator, ρ is the electrical resistivity, η is the Thomson coefficient, λ is the thermal conductivity, C is the specific heat, and $\mathbf{j}$ is the current density. It should be noted that the only term that may add bias to the temperature distribution around the crack plane is the Thomson heating effect. The sign of η controls the direction of the asymmetric temperature distribution.

Generally, the mass/vacancy diffusion is driven by the variation of chemical potential. The chemical potential can be represented by a function of the following local state variables

$$\mu = \mu(T, \sigma, X^\nu, \phi, \gamma), \qquad (3)$$

where σ is the stress tensor which defines the film stress state, X^ν is the vacancy concentration, ϕ is the electrical potential, and γ is the surface energy. Then the vacancy flux, $\mathbf{j}^\nu$, is defined through a general mobility tensor, $\mathbf{m}$:

$$\mathbf{j}^\nu = -\mathbf{m}\cdot\nabla\mu = -\mathbf{D}_{\text{soret}}\cdot\nabla T - \mathbf{D}_{\text{stress}}\cdot\nabla\sigma - \mathbf{D}\cdot\nabla X^\nu - Z^*|e|\mathbf{D}\cdot\nabla\phi - \mathbf{D}_{\text{surface}}\cdot\nabla\gamma, \qquad (4)$$

where $\mathbf{D}_{\text{soret}}$ is the Soret diffusion tensor, $\mathbf{D}_{\text{stress}}$ is the stress assisted diffusion tensor, $\mathbf{D}$ is the vacancies mobility tensor, e is the electron charge, Z^* is the effective valance of an atom, $Z^*|e|\mathbf{D}$ is the electromigration diffusion tensor and accounts also for the momentum transfer with the current carriers, and $\mathbf{D}_{\text{surface}}$ is the surface tension assisted diffusion. These diffusion

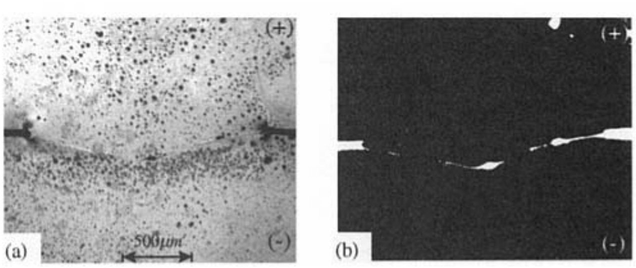

Fig. 9 Localized crack propagation in Au-film: (*a*) Reflected optical image; and (*b*) Transmitted optical image

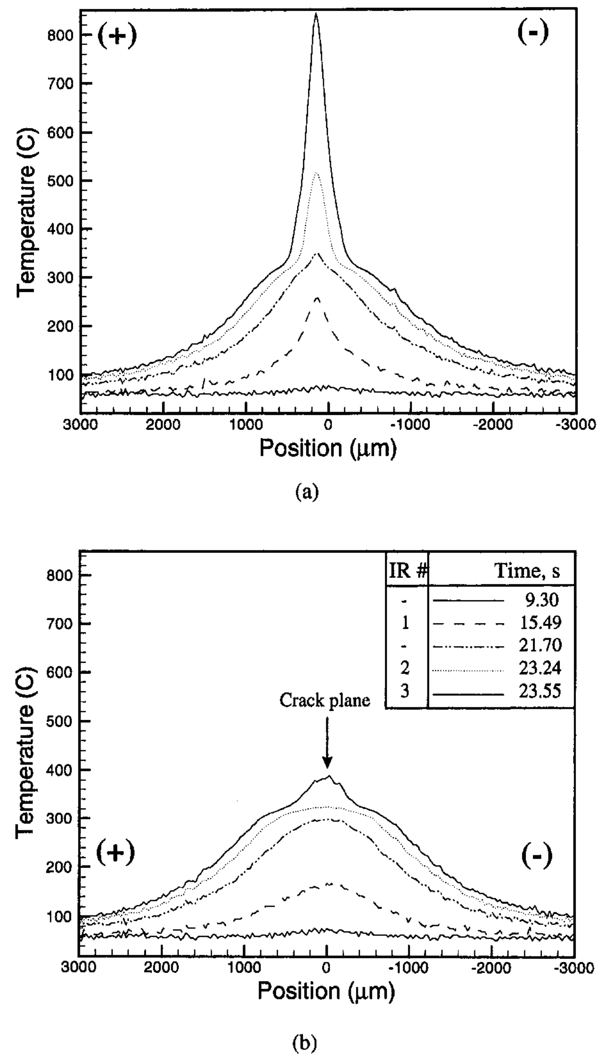

Fig. 10 Time dependent temperature distribution in Au-film: (*a*) tip temperature profile at line A-A of Fig. 8 up to the onset of crack propagation; and (*b*) middle plane temperature profile at line B-B of Fig. 8

tensors are temperature dependent. However, the exact dependence on temperature in the vicinity of melting is not well understood. Nevertheless, the various terms of Eq. (4) may be judged for possible dominating factors.

In the current experiments, stress assisted diffusion can be safely ignored since the tested lines were unpassivated. Surface tension assisted diffusion and diffusion caused by vacancy-concentration gradient do not provide bias in breaking the symmetry in crack growth. We believe that the failure pattern is mainly affected by the competition between electromigration and Soret diffusion. As seen from Eq. (2), the temperature distribution around the crack tip depends strongly on the biased Thomson effect. Thus, the competition between electromigration and Soret diffusion becomes the prime driving force for biasing the mass flux. It should be noted that detailed mechanisms of electromigration near melting temperature remain unknown.

In view of these assumptions, the crack-growth-mode failure of both the Al and Au films are believed to be primarily controlled by Soret diffusion. In aluminum, the crack propagates towards the positive electrode while piling material towards the negative electrode. These directions are against the direction of simple electromigration (Gardner et al., 1987). So, we inferred from the thermal measurements that at a current intensity rate of $\dot{K}^* \cong 5$ kA/cm$^{3/2}$, the crack propagation is due to Soret diffusion driven by a temperature gradient biased by a strong Thomson effect. When $\dot{K}^* \cong 0.5$ kA/cm$^{3/2}$, the local heat build up is reduced significantly due to heat conduction surpassing the heat generation rate. Therefore, electromigration becomes the prime driving force for grain boundary grooving within the uncracked ligament width as indicated in Fig. 3(a). At much faster loading rate $\dot{K}^* \geq 100$ kA/cm$^{3/2}$, an accelerated local heat build up ahead of the crack tip induces the localized failure in Fig. 3(c). For the gold film, the driving forces of electromigration and Soret diffusion are almost of the same order, resulting in the extended slit like failure between the two crack tips and slightly biased towards the negative electrode. Therefore, we concluded that Thomson effect has a slightly weaker influence on the failure process. The observed voids in the vicinity of the crack arise from the temperature gradient around the crack tip. It should be mentioned that, the existence of impurity ions might bias the direction of mass flux, in particular when using a substrate of a soda-lime glass. This biasing diffusion mechanism has not been investigated in this study.

The current study further ascertains the physical significance of the proposed current intensity rate $\dot{K}^*$, in controlling the competition between the various driving forces and the associated diffusion rates. Furthermore, the proposed failure criterion is successful in predicting the right order of magnitude of the total current to failure. It signifies the role of crack-like voids in accelerating the failure process because of the singular temperature and electric current density distributions. It should be noted that the proposed failure criterion has been tested for interconnect lines of much larger dimensions and much smaller grain size than those of practical use. However, the current toughness criterion, K_C^*, remains valid for a wide range of characteristic length scales, given a particular microstructure of a typical interconnect line.

Acknowledgments

A.-F. Bastawros would like to acknowledge the use of the High Resolution Thermo-Mechanical Measurements Facility at Harvard University. This work was supported in part by MRSEC program of the National Science Foundation under award No. DMR-9632524 at Brown University.

References

Adkins, C. J., 1983, *Equilibrium Thermodynamics*, Cambridge University Press, New York.

Attardo, M. J., and Rosenberg, R., 1970, ''Electromigration Damage in Aluminum Film Conductors,'' *Journal of Applied Physics*, Vol. 41, No. 6, pp. 2381–2386.

Bastawros, A.-F., and Kim, K.-S, 1995, ''Electro-Thermal Crack Growth Caused by Electric-Current Intensification,'' Proceedings, *Application of Fracture Mechanics in Electronic Packaging and Materials*, EEP-11/MD-64, ASME, New York, pp. 238–244.

Bastawros, A.-F., and Kim, K.-S, 1997, ''The Role of Electric-Current Induced Heating in Damage Evolution at the Crack Tip in Thin Films,'' Proceedings, *Application of Fracture Mechanics in Electronic Packaging*, EEP-20/AMD-222, ASME, New York, pp. 139–144.

EchoTherm Manual, 1997, Version 4.2, Thermal Wave Imaging Inc., Lathrup Village, MI.

Gardner, D. S., Meindl, J. D., and Saraswat, K. C., 1987, ''Interconnection and Electromigration Scaling Theory,'' *IEEE Transactions on Electron Devices*, ED-34, pp. 633–643.

Ho, P. S., 1970, ''Motion of Inclusion Induced by a Direct Current and a Temperature Gradient,'' *Journal of Applied Physics*, Vol. 41, pp. 64–68.

Marieb, T., Bravman, J. C., Flinn, P., and Madden, M., 1994, ''In Situ Observations of Voiding in Metal Lines Under Passivation,'' *Materials Research Society Symposium Proceedings 338*, pp. 409–413.

Saka, M., Sasagawa, K., and Abè, H., 1994, ''Theoretical Analysis of Electrothermal Crack Problem Considering Thomson Effect,'' Proceedings, ASME meeting, AMD-193, pp. 53–59.

Sigsbee, R. A., 1973, ''Electromigration and Metalization Lifetimes,'' *Journal of Applied Physics*, Vol. 44, No. 6, pp. 2533–2540.